Flow simulations of rectal evacuation: towards a quantitative evaluation from video defaecography

Faisal Ahmad, Stéphane Tanguy, Alain Dubreuil, Albert Magnin, Jean-Luc Faucheron, Clément de Loubens

Flow simulations of rectal evacuation: towards a quantitative evaluation from video defecography

Faisal Ahmad,[1] Stéphane Tanguy,[2] Alain Dubreuil,[3] Albert Magnin,[1] Jean-Luc Faucheron,[2,4] and Clément de Loubens[1]

[1] *Univ. Grenoble Alpes, CNRS, Grenoble INP, LRP, 38000 Grenoble, France*
[2] *Univ. Grenoble Alpes, CNRS, CHU Grenoble Alpes, Grenoble INP, TIMC, Grenoble, France*
[3] *Clinique du Mail, Grenoble, France*
[4] *Univ. Grenoble Alpes, CHU Grenoble Alpes, Colorectal Unit, Department of Surgery, Grenoble, France*

(Dated: August 22, 2022)

Mechanistic understanding of anorectal (patho)physiology is missing to improve the medical care of patients suffering from defecation disorders. Our objective is to show that complex fluid dynamics modeling of video defecography may open new perspectives in the diagnosis of defecation disorders. Based on standard X-ray video defecographies, we developed a bi-dimensional patient-specific simulation of the expulsion of soft materials, the feces, by the rectum. The model quantified velocity, pressure and stress fields during the defecation of a neostool with soft stool-like rheology for patients showing normal and pathological defecatory function. In normal defecation, the proximal-distal pressure gradient resulted from both the anorectal junction which formed a converging channel and the anal canal. The flow of the neostool through these anatomical parts was dominated by its shear-thinning viscous properties, rather than its yield stress. Consequently, the evacuation flow rate was significantly affected by variations in pressure applied by the rectum, and much less by the geometry of the anorectal junction. Lastly, we simulated impaired defecations in absence of obvious obstructive phenomena. Comparison with normal defecation allowed us to discuss critical elements which should lead to effective medical management.

I. INTRODUCTION

Defecation is a complex physiological process, which involves the coordination of neural, muscular, hormonal and cognitive systems [1]. It is triggered by abdominal contractions and thrusts during a Valsalva maneuver. The rectal evacuation is then relayed by the contraction of the rectal muscle that acts similar to the detrusor for bladder emptying [2]. Defecation disorders, which result in constipation or incontinence, are widespread in the worldwide population with prevalence in about 15% of the population [3, 4] and can significantly alter the quality of life of patients [5]. Because of the multi-factorial origins of defecation disorders and gaps in our understanding of normal and pathological defecation, it remains difficult for physicians to clearly distinguish etiologies from symptoms [6].

Defecation is the evacuation of soft materials, the feces, through the anorectal junction and the anal canal. There are many possible etiologies of defecation disorders, including, for example, slow bowel transit associated to hard feces difficult to expel, structural obstructive phenomena, anal sphincter injuries, etc. [1, 7]. It is also worth highlighting that a significant proportion of patients with impaired defecation do not have a well-defined anatomic disorder [8, 9]. Moreover, recent systematic characterization of defecographic abnormalities showed a strong overlap of structural and functional abnormalities in a large cohort of patients [16].

Although many testing tools are available to diagnose the anorectal function (manometry, video defecography, MRI, etc.), there are always some methodologic issues that limit the physicians' understanding of (patho)physiological defecations [10]. Discrepancies between tests are frequent and complicate the medical care of patients [11]. For example, manometry and evacuation are typically measured asynchronously under different conditions. Manometry is generally performed in non physiological conditions with an empty rectum, whereas evacuation is assessed with the expulsion of a balloon [12, 13]. To circumvent these limitations, researchers are developing and validating a soft core with embedded pressure sensors to combine manometry and defecography [14] Moreover, well established tests are partially processed. For example, video defecographies are currently used to assess structural and functional obstructive phenomena [1], although they contain physical information about the rectal function [8, 15]. All of these elements contribute to 'considerable controversy' in the coloproctology community regarding origins, consequences and treatment of patients [17–19].

In the context of this bleak epidemiology, there is strong agreement that efforts must be directed towards a mechanistic description of the defecatory function [1, 10]. Among the different gaps that have been identified in recent reviews [1, 10, 12], we focused in this paper on the modeling of the anorectal pressure forces generated during evacuation. Indeed, the relationships bettwen the pressure and the flow depends on (i) the anorectal geometry, (ii) the forces applied by the rectal muscles, (iii) the straining of the abdomen and (iv) the rheological properties of the feces. Feces is a yield stress fluid [20]. The yield stress of human feces varies naturally over several order of magnitudes depending on its water content [21]. When the stress applied is larger than the yield stress, feces flows as a shear thinning fluid [22–24]. Consequently,

we developed patient-specific simulations of rectal evacuation of yield stress fluids based on X-ray video defecographies with a neostool.

II. METHODS

The two dimensional (2D) patient-specific computational fluid dynamics (CFD) model of rectal evacuation was based on X-ray video defecographies [15]. Examinations were carried out in sitting position with a radio-opaque suspension (neostool) with soft stool-like rheology [8, 21, 25]. Rectal profiles were extracted to impose the kinetics of the rectum walls in the model. The algorithm was based on lattice-Boltzmann methods for yield stress fluids and moving boundary conditions. The CFD model simulated the evolution of velocity, pressure and stress fields in the rectal cavity.

A. Video defecographies

X-ray videodefecographies were carried out with the patient in sitting position, Fig. 1-a. The rectum was filled with a standardized radio-opaque neostool with a silicone gun [8, 25, 26] until the patient experienced rectal fullness, and visualized in the sagittal plane. Consequently, out-of-plane deformations could not be captured. However, such deformations are likely to happen in presence of anatomical abnormalities, which are easily observed in the sagittal plane [27]. As the orientation and z-location of the imaging plane could significantly affect the shape of the rectum, the position of the patient during the radiologic examination has been standardized, as well as the distance between the X-ray machine and the patient [8].

The radio-opaque neostool was prepared by mixing barium sulfate with a suspension of potato starch and cooked to obtain a paste with a yield stress τ_0 [8, 25]. The rheological properties of the neostool was characterized in our previous publication with standard rheometric techniques [21]. The relationships between the shear stress and the shear rate showed that the shear stress tends towards a constant value, the yield stress τ_0, when the shear rate tends towards 0, Fig. 1-b. This means that, as human feces, neostool can only flow if the stress applied is higher than the yield stress. The yield stress of the neostool was 350 Pa, which matched to the yield stress of soft regular human feces [21].

All the patients underwent X-ray defecographies during their health care pathways after they had complained of evacuation disorders, see Appendix A. The movies were selected among the examinations carried out in 2002 by A.D. Six X-ray videodefecographies were considered as representative of a normal evacuation of the neostool: the patients could evacuate the neostool without straining efforts and stool fragmentation, and had the sensation of a complete rectal evacuation. No developed anatomical abnormalities were observed and the function of the rectum and the anus was not considered pathologic after the examination. In agreement with an extensive quantification of normal evacuation in videodefecographies [15], 70 % of the standardised neostool had to be evacuated in one well-defined evacuatory attempt in less than 60 s. The 6 patients included 4 women of 60 to 80 years old

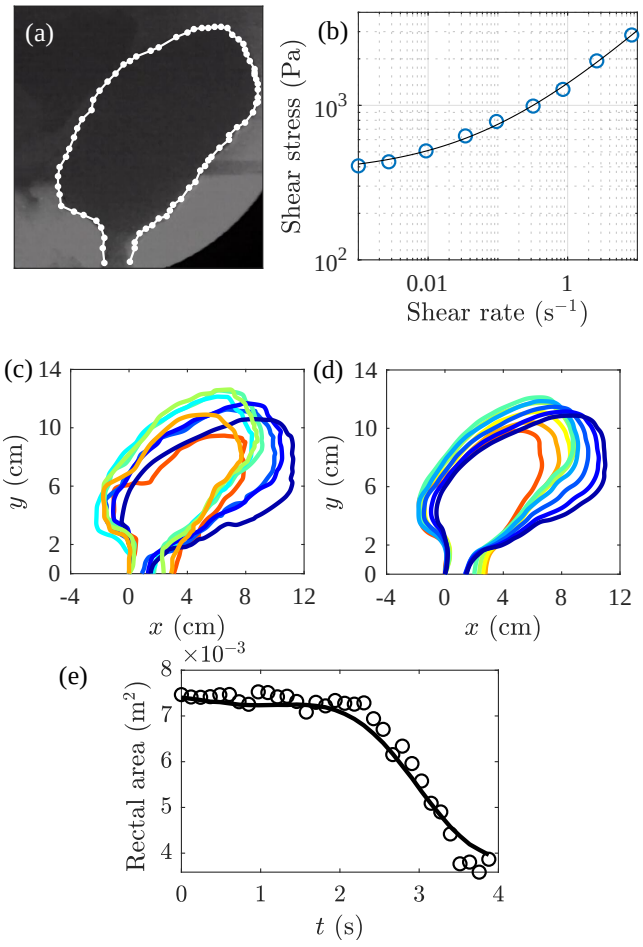

FIG. 1: X-ray defecography and image processing. *(a)* Sagittal view of the rectum filled with standardized radio-opaque neostool. White dots show the segmentation of the rectum. *(b)* Flow curve of the neostool (circles) fitted by the Herschel-Bulkley constitutive model for yield stress and shear-thinning fluids (plain line), from [21]. At low shear rate, the shear stress tends towards the yield stress. At high shear rate, the shear stress increases and the apparent viscosity decreases. *(c)* Raw profiles of the rectum after segmentation and interpolation for different time steps (time increasing from blue to red, patient N3). *(d)* Same profiles after smoothing. *(e)* Comparison of the area bounded by the raw boundaries (circles) and the smoothed boundaries (plain line) as a function of time t.

and 2 men of 55 and 80 year old. The length of the rectum (12 ± 5.5 cm), the angle between the anal canal axis and a tangent line to the posterior edge of the rectal ampulla (i.e. ano-rectal angle) at the beginning of the defecation (130 ± 22°) and the radius of the anal canal (0.95 ± 0.19 cm), were also in agreement with data reported by Palit *et al.* [15]. Data is reported as the mean ± the standard deviation.

As cases studies of functional defecation disorders, two videos (1 man and 1 woman) with abnormally slow rectal evacuation in the absence of visible anatomical abnormality, with the exception of a long anal canal and/or a closed anorectal angle at 90°, were also simulated. The quantity of neostool injected was standard (280 and 220 g).

Patients were informed that their anonymized data might in the future form the subject of clinical research and that they could object to this by informing the doctor. All procedures performed in this study complied with the requirements of the ethical standards research committee and with the Helsinki declaration. Ethics approval is not required for this retrospective study.

B. Flow modeling

The boundaries of the rectum were extracted from each video and processed as detailed in Appendix B. As a result of this process, the smoothed position of boundary nodes with equal arc length along the boundary of the rectum was obtained for each frame of the video (Fig. 1-c, d, e), along with the velocity $\mathbf{u_w}$ of each node. The mean outlet velocity V_a of the neostool through the anus is given by mass conservation, i.e.

$$V_a = \frac{1}{2R_a} \int_{\mathcal{L}} \mathbf{u_w}.\mathbf{n} \, \mathrm{d}l \tag{1}$$

where $\mathbf{n}$ is the normal to the boundary of the rectum, $\mathcal{L}$ is the contour length of the boundary and R_a is the radius of the anus.

As the neostool was very viscous and the Reynolds number very small, the flow was modelled using the incompressible Stokes equations in 2D for Herschel-Bulkley (HB) fluid. Mass and momentum equations are given by

$$\frac{\partial u_i}{\partial x_i} = 0, \; \frac{\partial \tau_{ij}}{\partial x_j} = \frac{\partial p}{\partial x_i} \tag{2}$$

where i,j (=1,2), u_i, x_i, τ_{ij} and p are the indices of the system of coordinates, the velocity, the coordinate, the viscous stress tensor and the pressure respectively. The relation between the viscous stress tensor τ_{ij} and the strain rate tensor $\dot{\gamma}_{ij} = \frac{\partial u_i}{\partial x_j}$ for the neostool was modelled by the HB constitutive equation

$$\begin{cases} \tau_{ij} = \left(\frac{\tau_0}{|\dot{\gamma}|} + k|\dot{\gamma}|^{n-1}\right)\dot{\gamma}_{ij}, & \text{if } |\tau| > \tau_0 \\ \dot{\gamma}_{ij} = 0, & \text{if } |\tau| \leq \tau_0 \end{cases} \tag{3}$$

where τ_0 is the yield stress, k the consistency index, n the flow index, $|\tau|$ and $|\dot{\gamma}|$ are the second invariant of each tensor. This set of equations was solved by lattice-Boltzmann methods, see details in Appendix C. The smoothed position of boundary nodes extracted from the video and their velocity $\mathbf{u_w}$ were used as boundary conditions along the moving wall of the rectum. The rheological parameters were fixed and determined by fitting the HB model on the flow curve of the neostool (plain line in Fig. 1-b): $\tau_0 = 350$ Pa, $n = 0.42$ and $k = 1000$ Pa.$s^{0.42}$.

Among the different physical quantities that we analysed, we also computed the stress applied in the normal direction by the fluid over the boundaries of the rectum, i.e the wall normal stress WNS, by

$$\mathrm{WNS} = (-p\mathbb{I} + \tau).\mathbf{n} \tag{4}$$

where $\mathbb{I}$ is the identity tensor. By integrating the WNS along the boundaries of the rectum, we calculated also the effective evacuation force $\mathbf{F}$ and its angle with the horizontal axis. $\mathbf{F}$ and the WNS are the resultant of both abdominal and rectal muscle contractions. We also systemically analyzed velocity, pressure and viscous stress fields. For brevity, the second invariant of the viscous stress tensor $|\tau|$ is refered as the viscous stress throughout this manuscript.

III. RESULTS

A. Normal defecations

For the six patients showing no signs of functional or anatomical pathologies, the outlet velocity of the neostool V_a could be characterized by one or two peaks, in agreement with extensive videodefecography studies [15]. We standardized the period of time during which the flow was simulated. This period of time was included between the two minima that framed the maximal outlet velocity V_a^{max}. The superposition of the profiles of the rectum shows that the proximal part of the rectum was squeezing the neostool through both the anorectal junction and the anal canal, Fig. 2-a. Both of these distal anatomical parts were static during the expulsive phase of defecation. In fact, the diameter of the anal canal showed little variation during the expulsive phase, $D_a = 2.0 \pm 0.4$ cm, whereas V_a^{max} increased up 9 ± 4 cm/s in a few seconds, Fig. 2-b. The color code in Fig.2-b shows the magnitude of the wall normal stress WNS. The WNS was maximal at the moving proximal part and decreased in the static anorectal junction.

Fields of velocity, pressure and viscous stress are shown in Fig. 3 at the time of maximum outflow velocity for

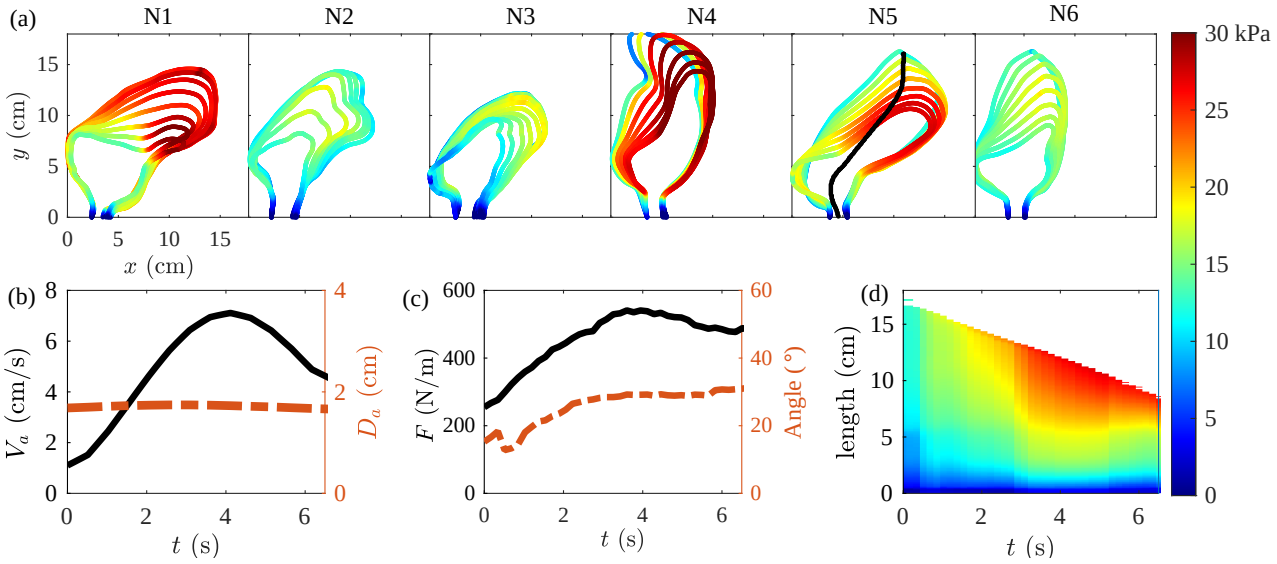

FIG. 2: Simulations of normal rectal evacuations through the open anal canal. *(a)* Evolution of the boundaries of the rectum during the evacuation of the neostool for 6 patients showing a normal rectal function. The color code shows the magnitude of the wall normal stress WNS. *(b)* Example of mean outlet velocity of the neostool through the anal canal V_a (plain lines, left axis) and diameter of the anal canal D_a (dashed lines, right axis) as a function of time (patient N5). *(c)* The evacuation force F (plain lines, left axis) and its angle with the y axis (dashed lines, right axis) as a function of time for patient N5 *(d)* Spatio-temporal map of the pressure variation along the length of a mid-line going from the anal canal (0 cm) to the proximal end at time 0 (black line in a-N5).

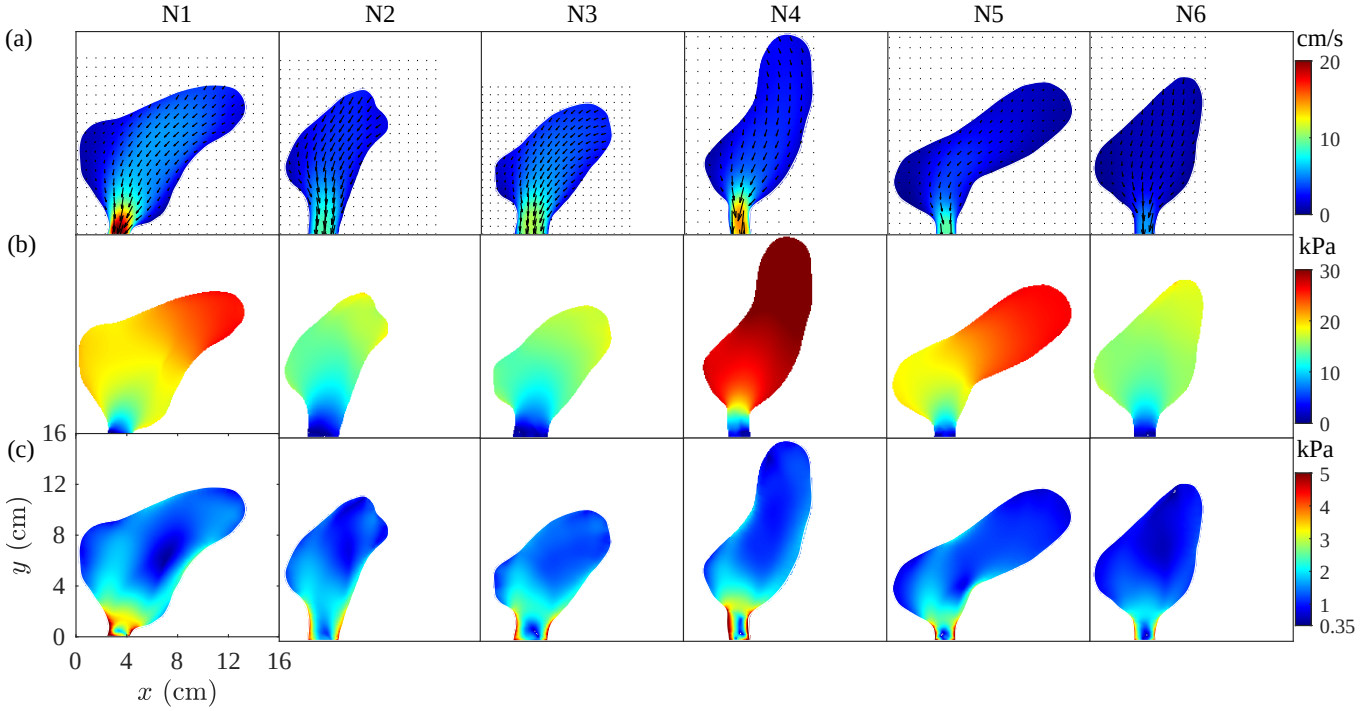

FIG. 3: Instantaneous *(a)* flow fields, *(b)* pressure fields and *(c)* viscous stress fields of 6 normal evacuations when the outlet velocity V_a was maximal.

each of the six patients. The velocity field was unidirectional and oriented along the mean curvature of the rectum, Fig. 3-a. Its magnitude was maximal in the anus. Some patients presented a small anterior pocket (typically patient 5), the so-called 'clubbing', in which the velocity was minimal. The pressure was maximal in the rectal ampulla, Fig. 3-b. Its gradient was mainly orientated along the mean curvature of the rectum. There was no pressure gradient in the radial direction wether in the rectal ampulla or in the anal canal. However, there was a gradient in the radial direction in the ano-rectal junction that formed a converging channel. The viscous stress was also maximal in the anus and the anorectal junction, Fig. 3-c. Its magnitude was greater than the yield stress of the neostool ($\tau_0 = 350$ Pa).

Similarly to high resolution manometry [28], the spatio-temporal (ST) evolution of the pressure along a mid-line going from the anal to the proximal ends (black lines on Fig. 2-a, N5) is shown for one typical example in Fig. 2-c. The map can be divided spatially and temporally. Spatially, in the rectal ampulla, the pressure was homogeneous and maximal (between 5 and 15 cm in Fig. 2-d). The maximum was approximately 25 kPa, i.e. an order of magnitude in agreement with rectal manometry values [28]. Between the beginning of the ano-rectal junction (at 5 cm) and the end of the anal canal (at 0 cm), the pressure dropped from 20 to 0 kPa. Temporally, the pressure was increasing and propagating towards the ano-rectal junction up to 3 s. A 3 s, the same level of pressure was maintained.

In all patients (N1-N6), the evacuation force **F** followed also a bell-shaped curve which was synchronized with the outlet velocity V_a (black lines on Fig. 2-b, c), whereas its angle α was almost constant during the evacuation (20 ± 13 °), which corresponded to the anorectal angle.

B. Abnormal defecations

The two patients showing functional pathology of rectal evacuation were characterized by the absence of structural obstructive phenomena [1], Fig. 4-a. However, for the first pathologic patient P1, the anal canal was almost twice longer than in normal patients and the anorectal angle was fully open. Conversely, for the patient P2, the anorectal angle was closed and the diameter of the anal canal was normally dilated. During the full examination which lasted about 2 min, there were different attempts of evacuation. We simulated the sequence corresponding to a successful and partial evacuation (12 and 30 s, respectively). The maximal outlet velocity through the anal canal $V_a \simeq 1$ cm/s was one order of magnitude lower than for normal evacuation, Fig. 4-b, black plain lines.

Fig. 5 shows velocity, pressure and viscous stress fields at the time of maximum outflow velocity. The flow was also unidirectional along the middle axis of the rectum. The organisation of the pressure field was also similar to that of normal patients, although its amplitude was twice lower. The pressure was almost homogeneous in the rectal ampulla for both patients. For P1, the pressure drop was significant in the anorectal junction and the anal canal (square in Fig.5-b). It was combined with a high

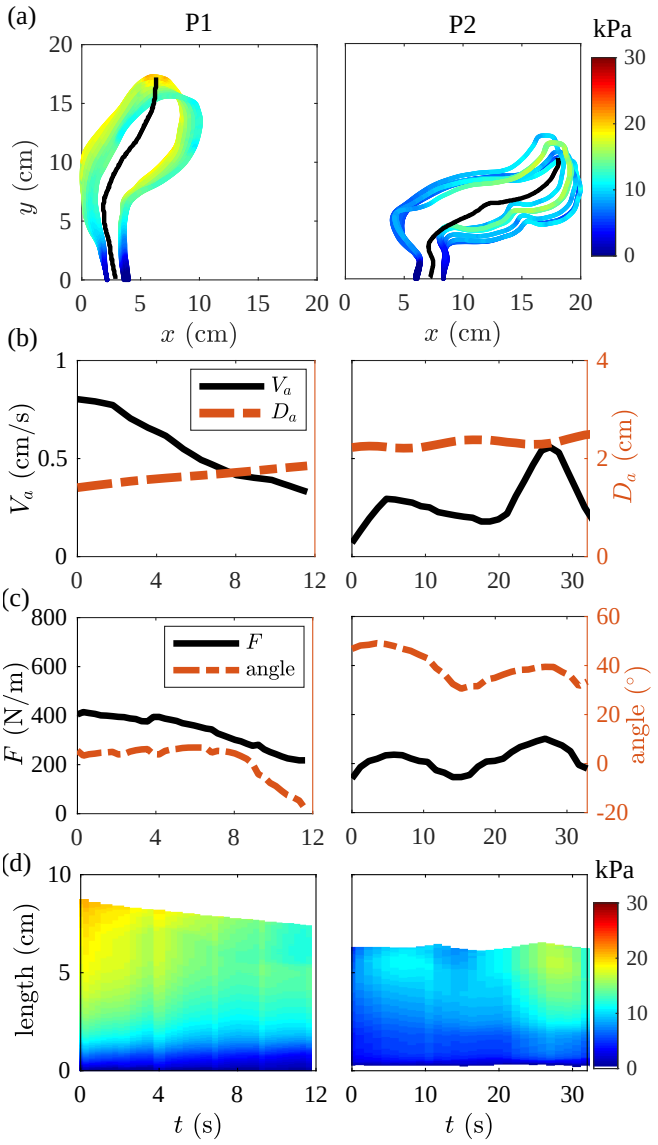

FIG. 4: Simulations of pathologic defecations showing abnormally slow evacuation. *(a)* Evolution of the boundaries of the rectum during the evacuation of the neostool for 2 patients. The color code shows the magnitude of the wall normal stress WNS. *(b)* Mean outlet velocity of the neostool through the anal canal V_a (plain lines, left axis) and diameter of the anal canal D_a (dashed lines, right axis) as a function of time. *(c)* The evacuation force F (plain lines, left axis) and its angle with the y axis (dashed lines, right axis) as a function of time. *(d)* Spatio-temporal map of the pressure variation along the length of mid-lines going from the anal canal (0 cm) to the proximal end (black lines in a).

viscous stress localized at the walls. For P2, the pressure drop was mainly localized in the 90° bend formed by the ano-rectal junction and the anal canal. In the anal canal, the viscous stress was also maximal at the walls. For both patients, the maximal viscous stress (2 kPa) was 3 times lower than for normal patients, Fig.5-c.

As for normal patients, the WNS was also maximal at the proximal part, Fig. 4-a. However, the movement of the boundaries was clearly limited. Fig. 4-c shows the ST-maps of pressure along the black lines displayed in Fig. 4-a. Again, there was a proximal to distal gradient. Lastly, the evacuation force F was coordinated with the outlet velocity V_a (black lines in Fig. 4-b, c). The maximal value ranged from 200 to 400 N/m which was to 2 to 3 times lower than for normal evacuation. The orientation of the force (dashed red lines in 4-c) was around 0° for P1 and 40° for P2.

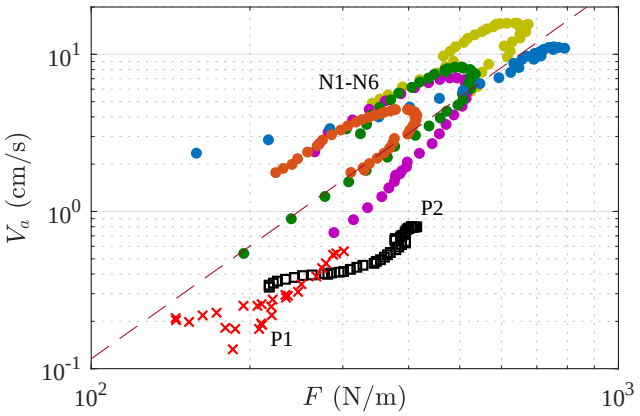

FIG. 6: Outlet velocity of the neostool through the anal canal V_a as a function of the force exerted by the rectum wall F for 6 normal (N1-N6, plain circles) and 2 pathologic (crosses and squares, P1-P2) evacuations. Dashed line is $V_a \sim F^{2.4}$.

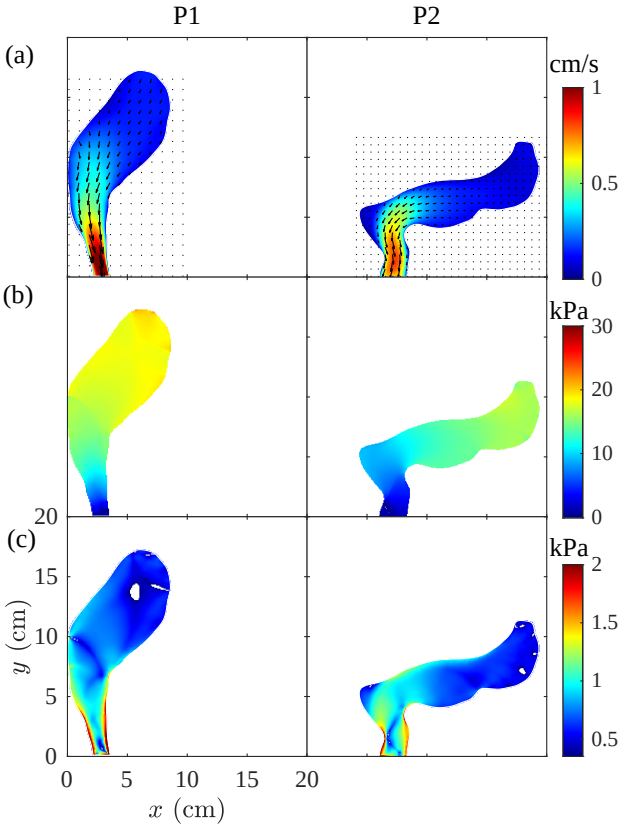

FIG. 5: Flow fields *(a)*, pressure fields *(b)* and viscous stress fields *(c)* of 2 pathologic evacuations when the mean outlet velocity of the neostool through the anal canal V_a was maximal. White color in *(c)* corresponds to regions where the viscous stress is lower than the yield stress of the neostool.

IV. DISCUSSION

The first attempts to model the fluid mechanics of human defecation were made by Farag [29, 30], who used the Hagen-Poiseuille law of purely viscous Newtonian fluids to deduce the intra-rectal pressure. Bush *et al.* [31] used a more realistic geometry by modeling the anorectal junction as a converging channel in the limit of purely plastic materials. In this asymptotic limit of the rheological behaviour of feces, the minimal pressure required to evacuate the feces is proportional to the yield stress [21] and a small change in the ratio of the diameters between the rectal ampulla and the anal canal can have a disproportionate effect on the flow resistance [21, 31]. Conversely, Yang *et al.* [24] considered that the flow of feces was solely governed by the rheology of the mucus layer and associated lubrication in a straight channel. This analysis was based on an observational study of defecation time across several animal species. To go beyond these speculations about the physical mechanisms that control rectal evacuation, we based our simulations on real anorectal kinetic data extracted from X-ray video defecographies and a full rheological model of the neostool. These simulations related pressure, stress and flow fields; these are fundamental quantities to understand flow phenomena and are impossible to obtain under physiological conditions with contemporary clinical investigation tests. Simulations give new insights into the fluid mechanics of human defecation, that we detailed below. Finally, we discuss how the assessment of pressure fields aid and guide the diagnosis of rectal evacuation disorders.

A. Fluid dynamics of normal defecation

Simulations of normal defecation showed that the viscous stress was always much larger than the yield stress of the neostool in the anal canal and the anorectal junction, by a factor of almost 10, Fig. 3-c. Moreover, pressure drops were also significant in these anatomical regions and negligible in the rectal ampulla, Fig. 2-d and 3-b, c. Consequently, the flow of the neostool was restricted by the anorectal junction and the anal canal and governed by its shear-thinning properties, rather than by its yield stress. Indeed, the Bingham number Bn, which is the ratio of yield stress to viscous stress, was of the order of 0.1 for normal evacuations;

$$Bn = \frac{\tau_0}{k}\left(\frac{R_a}{V_a^{max}}\right)^n \quad (5)$$

The pressure gradient was about 10 kPa/cm in both anatomical parts, Fig. 2-d and 3-a. We calculated analytically the pressure loss associated with both anatomical parts by considering that the neostool behaves as a shear-thinning fluid (i.e. $\tau_{ij} = k\dot{\gamma}_{ij}^n$, Appendix D). Pressure losses were $\simeq$ 15 kPa and $\simeq$ 6 kPa for the anus and the anorectal junction, respectively. These values were consistent with our simulations, and confirmed that both anatomical parts had a significant role on pressure losses. However, we assumed a 2D flow in our calculations. Based on analytical solutions of pressure loss in asymmetric converging channel [32], we expect that the pressure was underestimated by a factor 2 to 4 in our simulations. A fully quantitative evaluation of hydrodynamic parameters requires three dimensional modeling. These findings confirm the relevance of the simplified representation of the rectum introduced by Bush *et al.* [21, 31], who modelled the recto-anal junction as a converging channel.

Because of the shear-thinning properties of the neostool and human feces [21, 33], the relationship between the outlet velocity through the anal canal V_a and the evacuation force F was strongly non-linear. Based on the analytical solutions given in Appendix D for shear-thinning fluids, we expected that $V_a \sim F^{1/n}$. Fig. 6 shows V_a as a function of F for the six normal patients. Although the ascending part of defecation did not overlap with the descending part as the geometry was changing, the data was well fitted with a power law with $1/n = 2.4$, in agreement with the rheological properties of the neostool. This strongly non-linear relationship has an important consequence: small variations in force (pressure) lead to large variations in flow. When the force was multiplied by 3, the flow rate increased by a factor 10. Another important consequence of the shear-thinning behaviour is the weak variations in the pressure loss with the ratio of diameter between the rectal ampulla and the anal canal ($F \sim 1 - (D_r/D_a)^{-3n}$ in 3D, [32]). For example, if the ratio D_r/D_a is increased from 2 to 6, the pressure loss is multiplied by 1.6. Conversely, in the regime dominated by the yield stress, i.e. low velocity and/or high yield stress ($Bn >> 1$), F is very sensitive to the ratio of diameters ($F \sim \ln(D_r/D_a)$, [31]) and the pressure loss is multiplied by 2.5 if D_r/D_a increased from 2 to 6. As feces yield stress can be 22 times larger than the yield stress of the neostool [21], we can reasonably extrapolate that this asymptotic limit should be reached for hard feces, such as fecalom. In this case, the limiting factor would be the capacity of the anorectal musculature to dilate to a sufficient degree to allow defecation.

B. Towards a quantitative evaluation of pathophysiology of defecation

In the clinical practice, the prevalence of patients with functional and/or anatomical abnormalities is much higher than that of patients with normal defecography (85 vs. 15 %) [16]. We hypothesize that CFD modeling should help to find the origins of defecation disorders for patients showing anatomical and/or functional abnormalities, as it can measure simultaneously flow an pressure during defecation.

We illustrated how this data could be analyzed with two patients showing impaired defecations.

Patient P1, as a significant proportion of patients with impaired defecation [8, 9], had no well-defined anatomic disorders, Fig. 4-a. Simulated maximal pressure and forces were about 15 kPa and 300 N/m, almost twice smaller than in normal patients. Due to the non-linear pressure-flow relationship, the outlet velocity was 10 times lower than in normal patients. Red crosses in Fig. 6 show that this relationship for P1 followed the same power law than in normal patients at large forces ($F \sim V_a^{2.4}$) and was almost linear at small forces due to variations in the diameter of the anal canal. However, for the same F, V_a was twice smaller than in normal patients. This resulted from the fact that the anal canal was twice longer than for normal patients, and multiplying by 2 the pressure loss. The angle of the force was around 0 as the rectal ampulla and the anal canal were almost aligned. The Bingham number Bn was about 0.4, meaning that both the yield stress and the viscous effect control the dynamics of evacuation. This was also shown on the viscous stress field, which was of the same order of magnitude as the yield stress in the rectal ampulla and the anal canal. In conclusion, the main limited factor for this patient was an excessively weak applied pressure / force. This is in line with the concept of 'rectal akinesia'; the pathogenesis of which is a problem of rectal wall contractility [8, 9, 34]. Extending CFD simulations to video defecographies of patients showing impaired defecation in the absence of obvious obstructive phenomena should lead to a much better description of 'rectal akinesia'.

The second patient P2 did not present any obstructive phenomena, except an absence of variations in the anorectal angle which could be interpreted as a sign of anismus, also called dissynergic defecation. Anismus, a controversial topic [19, 35], is defined as inappropriate

contraction of the pelvic floor during attempted evacuation. The fluid mechanics parameters extracted from the simulations are similar to those of patient P1: maximal pressure (15 kPa) and force (400 N/m) twice smaller than in normal patients, Fig. 4 and black squares in Fig. 6. For both pathologic cases, we did not observe hysteresis in Fig. 6, contrarily to normal cases. It could be attributed to the fact that the shape of the recto-anal junction changed little over the course of defecation. The pressure drop was clearly associated with the flow of the neostool through the bend anorectal junction, Fig. 5-b. Consequently, the angle of the force was larger than for normal patients. However, as the pressure generated was smaller than in normal patients, we could postulate that the closed anorectal angle was not a cause of anorectal outlet obstruction. Thus, the existence of a dysfunction in the rectal wall contractility could be considered as a triggering factor of impaired defecation.

V. CONCLUSION

We introduced a fluid mechanics analysis of video defecography, which might be used to complete clinical investigations. Once applied to a large cohort of different types of patients, it should help physicians to better characterize the anorectal function and therefore, refresh our understanding of normal and pathologic defecation. In regard to the large overlap between functional and structural abnormalities in patients with defecation disorders [16], patient specific fluid mechanical simulations should help to identify the origin of these disorders. Specifically, they could help to identify reactoanal discoordination during excessive straining [36]. Finally, coupling medical imaging and complex fluid dynamics should contribute to a pathophysiological classification of evacuation disorders.

AUTHOR CONTRIBUTIONS

Faisal Ahmad: Investigation, Methodology, Software, Writing – original draft. **Stéphane Tanguy:** Conceptualization, Investigation, Methodology, Supervision, Validation, Writing – review & editing. **Alain Dubreuil:** Conceptualization, Investigation, Methodology, Resources, Validation, Writing – review & editing. **Albert Magnin:** Conceptualization, Validation, Writing – review & editing. **Jean-Luc Faucheron:** Conceptualization, Methodology, Resources, Writing – review & editing. **Clément de Loubens:** Conceptualization, Formal analysis, Funding acquisition, Investigation, Methodology, Software, Supervision, Writing – original draft.

DATA ACCESSIBILITY

Digitized raw X-ray video defecographies for each patient are given in Supplemental Materials.

FUNDING STATEMENT

LRP is part of the LabEx Tec21 (ANR-11-LABX-0030) and of the PolyNat Carnot Institute (ANR-11-CARN-007-01). The authors thank Agence Nationale de la Recherche for its financial support of the TransportGut project, ANR-21-CE45-0015.

[1] P. T. Heitmann, P. F. Vollebregt, C. H. Knowles, P. J. Lunniss, P. G. Dinning, and S. M. Scott, Understanding the physiology of human defaecation and disorders of continence and evacuation, Nature Reviews Gastroenterology & Hepatology **18**, 751 (2021).

[2] A. E. Bharucha and S. S. Rao, An update on anorectal disorders for gastroenterologists, Gastroenterology **146**, 37 (2014).

[3] P. D. Higgins and J. F. Johanson, Epidemiology of constipation in north america: a systematic review, Official journal of the American College of Gastroenterology—ACG **99**, 750 (2004).

[4] I. Ditah, P. Devaki, H. N. Luma, C. Ditah, B. Njei, C. Jaiyeoba, A. Salami, C. Ditah, O. Ewelukwa, and L. Szarka, Prevalence, trends, and risk factors for fecal incontinence in united states adults, 2005–2010, Clinical Gastroenterology and Hepatology **12**, 636 (2014).

[5] S. Perry, C. Shaw, C. McGrother, R. Matthews, R. Assassa, H. Dallosso, K. Williams, K. Brittain, U. Azam, M. Clarke, *et al.*, Prevalence of faecal incontinence in adults aged 40 years or more living in the community, Gut **50**, 480 (2002).

[6] S. M. Scott and M. A. Gladman, Manometric, sensorimotor, and neurophysiologic evaluation of anorectal function, Gastroenterology clinics of North America **37**, 511 (2008).

[7] A. E. Bharucha and B. E. Lacy, Mechanisms, evaluation, and management of chronic constipation, Gastroenterology **158**, 1232 (2020).

[8] J.-L. Faucheron and A. Dubreuil, Rectal akinesia as a new cause of impaired defecation, Diseases of the colon & rectum **43**, 1545 (2000).

[9] C. Morandi, J. Martellucci, M. Genovese, and P. Torricelli, Defecographic functional evaluation of rectal akinesia, Techniques in coloproctology **19**, 437 (2015).

[10] E. V. Carrington, S. M. Scott, A. Bharucha, F. Mion, J. M. Remes-Troche, A. Malcolm, H. Heinrich, M. Fox, and S. S. Rao, Advances in the evaluation of anorectal function, Nature reviews Gastroenterology & hepatology **15**, 309 (2018).

[11] S. Palit, N. Thin, C. H. Knowles, P. J. Lunniss, A. E. Bharucha, and S. M. Scott, Diagnostic disagreement between tests of evacuatory function: a prospective study of 100 constipated patients, Neurogastroenterology &

Motility **28**, 1589 (2016).
[12] B. Deb, M. Sharma, J. G. Fletcher, S. G. Srinivasan, A. Chronopoulou, J. Chen, K. R. Bailey, K. J. Feuerhak, and A. E. Bharucha, Inadequate rectal pressure and insufficient relaxation and abdominopelvic coordination in defecatory disorders, Gastroenterology **162**, 1111 (2022).
[13] K. Futaba, S.-C. Chen, W. W. Leung, C. Wong, T. Mak, S. Ng, and H. Gregersen, Fecobionics characterization of female patients with fecal incontinence, Scientific reports **12**, 1 (2022).
[14] H. Gregersen, K. Krogh, and D. Liao, Fecobionics: integrating anorectal function measurements, Clinical Gastroenterology and Hepatology **16**, 981 (2018).
[15] S. Palit, C. Bhan, P. Lunniss, D. Boyle, M. Gladman, C. Knowles, and S. Scott, Evacuation proctography: a reappraisal of normal variability, Colorectal Disease **16**, 538 (2014).
[16] U. Grossi, H. Heinrich, G. L. Di Tanna, S. A. Taylor, P. F. Vollebregt, C. H. Knowles, and S. M. Scott, Systematic characterization of defecographic abnormalities in a consecutive series of 827 patients with chronic constipation, Diseases of the Colon & Rectum **64**, 1385 (2021).
[17] A. Zbar, M. Guo, and M. Pescatori, Anorectal morphology and function: analysis of the shafik legacy, Techniques in coloproctology **12**, 191 (2008).
[18] R. Lentle and P. Janssen, Physical characteristics of digesta and their influence on flow and mixing in the mammalian intestine: a review, Journal of Comparative Physiology B **178**, 673 (2008).
[19] W. Schouten, J. Briel, J. Auwerda, J. Van Dam, M. Gosselink, A. Ginai, and W. Hop, Anismus: fact or fiction?, Diseases of the colon & rectum **40**, 1033 (1997).
[20] N. J. Balmforth, I. A. Frigaard, and G. Ovarlez, Yielding to stress: recent developments in viscoplastic fluid mechanics, Annual Review of Fluid Mechanics **46**, 121 (2014).
[21] C. de Loubens, A. Dubreuil, R. G. Lentle, A. Magnin, N. E. Kissi, and J.-L. Faucheron, Rheology of human faeces and pathophysiology of defaecation, Techniques in Coloproctology **24**, 323 (2020).
[22] P. Patel, B. Picologlou, and P. Lykoudis, Biorheological aspects of colonic activity, Biorheology **10**, 441 (1973).
[23] S. Woolley, R. Cottingham, J. Pocock, and C. Buckley, Shear rheological properties of fresh human faeces with different moisture content, Water SA **40**, 273 (2014).
[24] P. Yang, M. Lamarca, C. Kaminski, D. Chu, and D. Hu, Hydrodynamics of defecation., Soft matter **13 29**, 4960 (2017).
[25] P. Mahieu, J. Pringot, and P. Bodart, Defecography: I. description of a new procedure and results in normal patients, Gastrointestinal radiology **9**, 247 (1984).
[26] J. Faucheron, S. Barot, D. Collomb, N. Hohn, D. Anglade, and A. Dubreuil, Dynamic cystocolpoproctography is superior to functional pelvic magnetic resonance imaging in the diagnosis of posterior pelvic floor disorders: results of a prospective study, Colorectal Disease **16**, 240 (2014).
[27] V. Ratz, T. Wech, A. Schindele, A. Dierks, A. Sauer, J. Reibetanz, A. Borzi, T. Bley, and H. Köstler, Dynamic 3d mr-defecography, in *RöFo-Fortschritte auf dem Gebiet der Röntgenstrahlen und der bildgebenden Verfahren*, Vol. 188 (© Georg Thieme Verlag KG, 2016) pp. 859–863.
[28] E. V. Carrington, A. Brokjaer, H. Craven, N. Zarate, E. Horrocks, S. Palit, W. Jackson, G. Duthie, C. Knowles, P. Lunniss, *et al.*, Traditional measures of normal anal sphincter function using high-resolution anorectal manometry (hram) in 115 healthy volunteers, Neurogastroenterology & Motility **26**, 625 (2014).
[29] A. Farag, Use of the hagen-poiseuille law: A new mathematical approach for the integration and evaluation of anorectal physiological testing in patients with faecal incontinence and pelvic dyschezia and in normal controls, European Surgical Research **30**, 279 (1998).
[30] A. Farag, The use of flow equation in functional coloproctology: a new theory in anorectal physiology (Galenos Publishing House, 2009) p. 17.
[31] M. Bush, P. Petros, M. Swash, M. Fernandez, and A. Gunnemann, Defecation 2: Internal anorectal resistance is a critical factor in defecatory disorders, Techniques in coloproctology **16** (2012).
[32] R. Lenk, Pressure drop through tapered dies, Journal of Applied Polymer Science **22**, 1775 (1978).
[33] R. Penn, B. J. Ward, L. Strande, and M. Maurer, Review of synthetic human faeces and faecal sludge for sanitation and wastewater research, Water research **132**, 222 (2018).
[34] R. L. Grotz, J. H. Pembérton, K. E. Levin, A. M. Bell, and R. B. Hanson, Rectal wall contractility in healthy subjects and in patients with chronic severe constipation., Annals of surgery **218**, 761 (1993).
[35] L. Gottesman, Anismus through surgical eyes, Diseases of the Colon & Rectum **65**, 137 (2022).
[36] A. Picciariello, P. O'Connell, D. Hahnloser, G. Gallo, A. Munoz-Duyos, O. Schwandner, P. Sileri, G. Milito, S. Riss, P. Boccasanta, *et al.*, Obstructed defaecation syndrome: European consensus guidelines on the surgical management, British Journal of Surgery **108**, 1149 (2021).
[37] S. Chaussade, A. Khyari, H. Roche, M. Garret, M. Gaudric, D. Couturier, and J. Guerre, Determination of total and segmental colonic transit time in constipated patients, Digestive diseases and sciences **34**, 1168 (1989).
[38] I. Ginzburg, F. Verhaeghe, and D. d'Humieres, Two-relaxation-time lattice boltzmann scheme: About parametrization, velocity, pressure and mixed boundary conditions, Communications in computational physics **3**, 427 (2008).
[39] D. Rui and B.-c. Shi, Incompressible multi-relaxation-time lattice boltzmann model in 3-d space, Journal of Hydrodynamics, Ser. B **22**, 782 (2010).
[40] L. Talon and D. Bauer, On the determination of a generalized darcy equation for yield-stress fluid in porous media using a lattice-boltzmann trt scheme, The European Physical Journal E **36**, 139 (2013).
[41] T. Papanastasiou and A. Boudouvis, Flows of viscoplastic materials: models and computations, Computers & Structures **64**, 677 (1997).
[42] D. d'Humières and I. Ginzburg, Viscosity independent numerical errors for lattice boltzmann models: From recurrence equations to "magic" collision numbers, Computers & Mathematics with Applications **58**, 823 (2009).
[43] S. Gsell, U. D'Ortona, and J. Favier, Lattice-boltzmann simulation of creeping generalized newtonian flows: Theory and guidelines, Journal of Computational Physics , 109943 (2020).
[44] P. Lallemand and L.-S. Luo, Lattice boltzmann method for moving boundaries, Journal of Computational Physics **184**, 406 (2003).

[45] S. Gsell, U. d'Ortona, and J. Favier, Lattice-boltzmann simulation of creeping generalized newtonian flows: Theory and guidelines, Journal of Computational Physics **429**, 109943 (2021).

[46] Y. Wang, J. G. Brasseur, G. G. Banco, A. G. Webb, A. C. Ailiani, and T. Neuberger, Development of a lattice-boltzmann method for multiscale transport and absorption with application to intestinal function, in *Computational modeling in biomechanics* (Springer, 2010) pp. 69–96.

Appendix A: Video defecographies

All the patients with normal radiologic evacuation had no particular severe medical or surgical history except a nervous breakdown treated by anti-depressive drugs in a female patient aged 67 who also had anal incontinence, a hysterectomy for benign disease in a patient aged 64, and an anal incontinence in a female patient aged 61. These 6 patients presented with transit time constipation confirmed by a transit time examination [37] that responded to laxatives in 4 days; and all were referred to the radiologist (AD) for suspicion of pelvic floor disorder because they complained from dyschesia that responded to suppositories, enemas, and/or digital maneuvers for rectal evacuation. At that time, no specific obstructive defecation syndrome had been published [36].

Two further patients (one female and one male) with no particular past medical or surgical history presented with absence of pelvic organ deformity during defecation, but were suspected to suffer from rectal akinesia [26] in one and anismus (also called recto-anal dyssynergia) in the other [19].

Appendix B: Video processing

X-ray analog images (HI-8) were first digitized using VLC media player software and then processed with the Image Processing Toolbox of Matlab R2019b (Mathworks). The boundaries of the rectum and the anus were manually segmented with at least 40 points for each image. The coordinates of the boundary were interpolated with a Piecewise Cubic Hermite Interpolating Polynomial (PCHIP) method to increase the spatial resolution. Boundary nodes with equal arc-length distance were sampled from the interpolated boundary. The coordinates of these extracted nodes were spatially and temporally smoothed with a 2D Gaussian filter. This step permitted also to remove mass movements of the rectum when the patient was moving. The smoothed set of data was linearly interpolated for subsequent CFD simulations and differentiateed to deduce the velocity of each node of the boundary. In order to validate the image processing algorithm, for each patient, the variations in the surface area bounded by the smoothed boundaries were compared to the one bounded by the raw data, Fig. 1-e.

Appendix C: Lattice-Boltzmann methods

D2Q9 incompressible BGK lattice-Boltzmann methods with two relaxation times were used to simulate the creeping flow of a yield stress fluid with the Herschel-Bulkley constitutive equation during rectal emptying [38–40]. The nine discrete velocities are defined by,

$$\mathbf{e}_\alpha = (0,0)\,,\ \text{for } \alpha = 0$$

$$\mathbf{e}_\alpha = (\pm c, 0)\,, (0, \pm c)\,,\ \text{for } \alpha = 1-4$$

$$\mathbf{e}_\alpha = (\pm c, \pm c)\,, (\pm c, \pm c)\,,\ \text{for } \alpha = 5-8$$

where $c = \Delta x/\Delta t$, Δx and Δt are the lattice grid spacing and lattice time step respectively. The evolution equation of the model is divided into two steps, the propagation,

$$f_\alpha\left(\mathbf{x} + \mathbf{e}_\alpha \Delta t, t + \Delta t\right) = \hat{f}_\alpha$$

and the collision,

$$\begin{aligned}\hat{f}_\alpha\left(\mathbf{x}, t\right) = &\frac{1}{\tau_+}\left[f_\alpha^+\left(\mathbf{x}, t\right) - f_\alpha^{+,eq}\left(\mathbf{x}, t\right)\right] \\ &+\frac{1}{\tau_-}\left[f_\alpha^-\left(\mathbf{x}, t\right) - f_\alpha^{-,eq}\left(\mathbf{x}, t\right)\right]\end{aligned}$$

$$f_\alpha^+ = \frac{1}{2}\left(f_\alpha + f_{\bar{\alpha}}\right),\ f_\alpha^- = \frac{1}{2}\left(f_\alpha - f_{\bar{\alpha}}\right)$$

$$f_\alpha^{+,eq} = \frac{1}{2}\left(f_\alpha^{eq} + f_{\bar{\alpha}}^{eq}\right),\ f_\alpha^{-,eq} = \frac{1}{2}\left(f_\alpha^{eq} - f_{\bar{\alpha}}^{eq}\right)$$

where f_α is the density distribution function, f_α^{eq} is the equilibrium distribution function, symbols '+' and '−' refer to the symmetric and anti-symmetric part of both functions, $\bar{\alpha}$ is the opposite direction to α (i.e $\mathbf{e}_\alpha = -\mathbf{e}_{\bar{\alpha}}$), τ_+ and τ_- are the two relaxation parameters, $\hat{f}$ is the density distribution function after collision and before propagation. f_α^{eq} is defined as

$$f_\alpha^{eq} = \begin{cases} 1 - (1-\omega_0)\frac{p}{c_s^2} + s_0(u), & \alpha = 0 \\ \omega_\alpha \frac{p}{c_s^2} + s_\alpha(\mathbf{u}), & \alpha = 1-8 \end{cases}$$

where $s_\alpha(\mathbf{u}) = 3\omega_\alpha e_\alpha \cdot \mathbf{u}$, for Stokes flow, $c_s = 1/\sqrt{3}$ is the speed of sound. The weight coefficients are given by

$$w_\alpha = \begin{cases} 4/9, & \alpha = 0 \\ 1/9, & \alpha = 1,2,3,4 \\ 1/36, & \alpha = 5,6,7,8 \end{cases}$$

The macroscopic flow velocity and pressure are computed from the distribution functions,

$$\mathbf{u} = \sum_{\alpha=1}^{8} e_\alpha f_\alpha$$

$$p = \frac{c_s^2}{1-\omega_0}\left[\sum_{\alpha=1}^{8} f_\alpha + s_0(\mathbf{u})\right]$$

The rate-of-strain ($\dot{\gamma}_{ij}$) tensor is given by

$$\dot{\gamma}_{ij} = -\frac{1}{2c_s^2\tau_+\Delta t}\sum_{i=0}^{18}\mathbf{e}_{i\alpha}\mathbf{e}_{i\beta}\left[f_i^+(\mathbf{x},t) - f_i^{+,eq}(\mathbf{x},t)\right]$$

The local viscosity was calculated with the Papanastasiou regularization of the Herschel-Bulkley consitutive equation by [40, 41]

$$\eta = \frac{\tau_0}{|\dot{\gamma}|}[1-\exp(-m|\dot{\gamma}|)] + k|\dot{\gamma}|^{n-1}$$

where $|\dot{\gamma}| = \sqrt{\dot{\gamma}_{ij}\dot{\gamma}_{ij}}$ is the second invariant of the rate-of-strain tensor and m the regularization coefficient. The symmetric relaxation time (τ_+) was calculated using

$$\tau_+ = \frac{6\eta+1}{2}$$

The anti-symmetric relaxation parameter is defined by

$$\tau_- = \frac{\Lambda}{\tau_+ - 0.5} + 0.5$$

where Λ is the magic collision parameter and taken to 1/4 in order to optimize the accuracy of the numerical scheme [42]. The TRT-LBM scheme was used as it is superior to the standard single relaxation time LBM scheme because it avoids strong numerical errors for non-Newtonian flows with large variations in viscosity [40, 43].

No-slip and moving boundary conditions were treated with a combination of the bounce-back scheme and the transfer of momentum to the fluid due the velocity of moving boundary ($\mathbf{u_w}$), see [44] for details. Outlet velocity was also imposed at the end of the anus. For each time step, the mean flow rate was known from image analysis and the flow profile was given by the analytical solution of the 2D Poiseuille flow for a Herschel-Bulkley fluid [40].

To solve the flow, we used the time-independent property of Stokes flow equations (Eq. 2) to speed-up the algorithm. For each movie, the time sequence of rectal emptying was divided into 40 time steps. For each time step, the corresponding boundary conditions were applied. The collision and streaming operations were computed. The local effective viscosity was updated. The iteration was pursued until convergence of the flow field was reached. It was repeated for each of the 40 time steps.

This methodology was already validated to solve flow of yield stress fluids [40, 45]. We validated the code with benchmarks, such as Poiseuille flow [40] or flow past a fixed/moving cylinder [46]. The grid to solve the flow consisted of about 4000 lattices. The value of m was chosen after preliminary tests and is a compromise between precision and speed of convergence. Excessively low values of m result in poor consideration of yield stress effects in the simulation, while excessively high values result in the code taking too long to converge.

Appendix D: Pressure loss in simplified geometries

Analytical solutions used to calculate the pressure loss for shear-thinning fluids in a 2D converging channel and in a straight channel were developed by Lenk [32] which read

$$\Delta P1 = \frac{k\cot\theta}{n}\left(Q\left(4n+2\right)\right)^n H_2^{-2n}\left[1-\left(\frac{H_1}{H_2}\right)^{-2n}\right]$$

for the converging channel, where θ is the vertical taper angle, Q is the flow rate, H_1 and H_2 are the width at inlet and outlet of the converging channel and

$$\Delta P2 = \frac{2Lk}{h^{2n+1}}\left(Q\frac{4n+2}{n}\right)^n$$

for the straight channel, with h its width. Note that the analytical solution for the converging channel is valid for small angles θ ($< 15°$) and we extrapolated the formula to a larger angle (45°) so as to calculate orders of magnitude of pressure loss in the anorectal junction.